V European Conference on Computational Fluid Dynamics
ECCOMAS CFD 2010
J. C. F. Pereira and A. Sequeira (Eds)
Lisbon, Portugal,14-17 June 2010

LARGE EDDY SIMULATION OF FORCED IGNITION IN HIGHLY STRAINED BLUFF-BODY BURNER

V. Subramanian*, P. Domingo* and L. Vervisch*

*CORIA-CNRS and INSA de Rouen, Campus de Madrillet
Avenue de l'Université, BP 8, 76801 Saint Etienne du Rouvray Cedex, France
e-mail: pascale.domingo@coria.fr

Key words: Large Eddy Simulations, Spark ignition, Non-premixed turbulent flames

Abstract. *Large Eddy Simulation (LES) of forced ignition is performed using tabulated detailed chemistry. The objective is to reproduce the flame properties observed in a recent experimental work, reporting probability of ignition in a laboratory-scale burner operating with Methane/air non premixed mixture (Combust. Flame 151 (2007) 366–385). The smallest scales of chemistry are approximated with a flamelet model combined with presumed probability density functions, to account for turbulent fluctuations of species and temperature that are not resolved by the LES grid. One-dimensional flamelets are first computed with detailed chemistry and tabulated under a set of parameters describing the local mixing and progress of reaction. Spark ignition is mimicked on selected ignition spots and the dynamics of kernel development analyzed and compared against the experimental observations. The possible link between the success or failure of the ignition and the flow conditions (in terms of velocity and composition) at the sparking time are then explored. It is shown that neglecting strain rate effects in chemistry tabulation does not allow for reproducing all the subtleties of experimental observations and a novel closure is discussed to overcome these limitations.*

1 INTRODUCTION

Growing interest in optimization of aeronautical engine relight in high altitude motivates studies of non-premixed burner forced ignition. The forced ignition phenomenon observed in such burners are highly transient in nature. Various factors influence the development of spark kernel from the moment of spark deposit, until the complete flame establishment period. A three dimensional LES computation is performed to analyze the spark ignition kernel development in a turbulent flow field behind a conical shaped bluff-body non-premixed burner. The experimental target of this simulation is the ignition experiment conducted by Ahmed et al [1]. A conventional flamelet approach is combined with presumed beta-shape pdf to account for unresolved sub-grid scale phenomena. Unstrained flamelets allows for representing with accuracy all the experimentally observed

types of flame development after sparking at locations situated outside the central recirculation zone (CRZ). However, the weak probability of ignition success when the spark is located inside the CRZ cannot be captured. In the experiment, at this location, the kernel has a tendency to exhibit serious shrinkage following spark and subsequently disappears. This behavior was attributed in the experiment to high level of strain rate acting on a kernel developing in a fuel rich mixture. The shortcoming of the modelling approach is then mainly due to the fact that the technique is constructed based on unstrained laminar flamelet calculations and so, the effect of aerodynamic strain on detailed chemistry is neglected in the model closure. The failure due to aerodynamic strain are thus not reproducible in the simulation. To overcome this limitation, a correction to the tabulated filtered burning rate sources coming from conventional flamelet table is proposed based on the intensity of the local rate of strain. The stretch is accounting for in a global manner, with a first order strain rate correction function based on one-dimensional laminar flamelet response to strain. The correction function mimics the reduction in burning rate from the local LES resolved strain rate and is also a function of local equivalence ratio. This correction, whose impact is more important in the fuel rich CRZ, leads to an improved combustion model that reproduces the quenching of flame kernels undergoing intense local stretch. Nevertheless, successful ignition event are still observed in and outside the CRZ, with the proposed correction factor ensuring that the new model is not artificially over-dampening.

2 SGS MODELING

2.1 FLOW SOLVER

Computations are performed with a finite volume formulation in a collocated grid using the LES nonpremixed turbulent flame methodology proposed by Domingo *et al.* [2], which is based on tabulated detailed chemistry and presumed sub-grid scale (SGS) probability density functions, coupled with the solving of the fully compressible form of the Navier-Stokes balance equations of mass, momentum and energy. The domain, corresponding to the experimental enclosure [1], measures 70 mm in spanwise direction and 80 mm in streamwise direction, it is discretized over 1,764,000 grid points. The grid is uniform in spanwise direction and slightly stretched in the streamwise direction near the inlet, to capture the flow in the intense turbulence region near the bluff body lip. Implicit filtering is used in this LES and the characteristic size of the LES mesh is of the order of 0.4 mm. A series of twenty simulations with different sparking cases have been completed and analyzed. A fourth order skew symmetric like scheme [3] is adopted for convective terms, while fourth order centred scheme is employed for diffusive flux calculations. Time marching is done with explicit minimum storage Runge-Kutta scheme of order three [4]. The annular inflow of air and fuel are constructed from hyperbolic tangent profiles at the inlet plane, matching the corresponding experimental mass flow rates.

The inflow mean velocities are superimposed with synthetic turbulence, generated from

the procedure proposed by Klein *et al.* [5]. Symmetric boundary conditions are applied at the spanwise boundaries (there is a wall enclosure in the experiment far from the axis of symmetry of the burner), and, non-reflecting subsonic outflow boundary condition is used at the outlet boundary. Acoustic waves travelling in and out of the computational domain were treated based on the Navier-Stokes characteristics Boundary condition (NSCBC) [6].

Transport by unresolved velocity fluctuations are expressed using Smagorinsky [7] closure; the maximum eddy viscosity never exceeds 20 times the molecular viscosity. Realistic thermochemical effects are included by considering the specific heat capacity as a function of temperature as well as composition. The species mass fractions (N_2, CH_4, O_2, CO_2, H_2O, CO, H_2, OH) needed to obtain a correct estimation of the temperature [8] are tabulated, as now discussed.

2.2 SGS COMBUSTION MODELING

Various methods have been proposed to tabulate the high complexity of combustion chemistry, to keep LES computing requirements sufficiently low. One approach consists of considering canonical laminar combustion model problems, so-called flamelets, which are filtered with presumed pdfs to account for unresolved sub-grid scale fluctuations, it is named here PCM-FPI [9, 10]; details concerning the background of this modeling approach applied to LES may be found in [11, 2, 8, 12]. Two versions of SGS modeling are discussed in this paper, the first one does not account for the impact of flame stretching on the burning rate of the reference flamelets, the second includes a stretch correction. Premixed laminar flamelets are considered, mainly for three reasons: (i) the turbulent mixing rate is high in this burner and sparking occurs in already mixed reactants; (ii) once the burning kernel formed after energy deposit, partially premixed flame propagation may play some role in flame spreading, (iii) it was shown in previous studies, that most of non-premixed combustion properties in terms of energy release are reproduced by premixed flamelet tabulation, at least for equivalence ratio below 1.8 [13, 2].

Space filtered quantities are denoted $\overline{\varphi}(\underline{x},t)$, the mass weighted filtered scalars and chemical source terms read,

$$\overline{\rho}\widetilde{\varphi} = \overline{\rho\varphi} = \overline{\rho}\int_0^1 \left(\overline{\varphi \mid Z^*;\underline{x},t}\right)\widetilde{P}(Z^*;\underline{x},t)\,dZ^* \tag{1}$$

where ρ is the density and $\left(\overline{\varphi \mid Z^*;\underline{x},t}\right)$ is the filtered conditional mean of φ, estimated for the mixture fraction value $Z = Z^*$ (a passive scalar verifying $Z = 0$ in air and $Z = 1$ in fuel jet); $\widetilde{P}(Z^*;\underline{x},t)$ is the mass weighted filtered probability density function of mixture fraction Z, presumed to take a Beta shape. The chemistry evolution is projected in a low-dimensional composition space, which is here reduced to two variables, Z and a reaction progress variable Y_c, built from the sum of CO and CO_2 mass fractions, ensuring a one-to-one correspondence between Y_c and species concentrations and sources [14, 15]. A normalized progress variable is also defined, as Y_c normalized by its equilibrium value

$c = Y_c/Y_c^{Eq}$, where Y_c^{Eq} is determined with EQUIL software [16]. The filtered conditional mean is then given as:

$$\left(\overline{\varphi \mid Z^*;\underline{x},t}\right) = \int_0^1 \int_{K-}^{K+} \varphi^{FPI}(Z^*,c^*,K^*)\overline{P}(c^*;\underline{x},t)\overline{P}(K^*;\underline{x},t)\,dc^*dK^* \tag{2}$$

where, φ^{FPI} is a scalar or a source term arising from the flamelets calculations and $\overline{P}(c^*;\underline{x},t)$ is the filtered probability density function of normalised progress of reaction, which is also presumed to follow a Beta distribution. $\overline{P}(K^*;\underline{x},t)$ is the flame stretch pdf [17, 18, 19] whose statistical space covers $[K-,K+]$; in a first analysis c and K can be assumed statistically independent [19]. The two marginal pdfs $\widetilde{P}(Z^*;\underline{x},t)$ and $\overline{P}(c^*;\underline{x},t)$ are presumed from $\widetilde{Z}$, $Z_v = \widetilde{ZZ} - \widetilde{Z}\widetilde{Z}$, $\widetilde{Y}_c$ and $\widetilde{Y_cY_c}$ for which balance equations are solved [2]; the hypothesis of statistical independence between Z and c (not Y_c) was previously discussed [9, 2]. $\widetilde{Y_c^2}$ is solved instead of the SGS variance for numerical reasons, to avoid transporting the energy of the resolved field $\widetilde{Y_c}^2$ within the SGS variance [11, 20].

Scalar dissipation rates appear in the equations for Z_v and $\widetilde{Y_cY_c}$ [2], they measure the SGS turbulent mixing rate and are decomposed into their resolved and SGS parts:

$$\overline{\rho}\widetilde{\chi}_\varphi = \overline{\rho\mathcal{D}|\nabla\varphi|^2} = \overline{\rho}\mathcal{D}|\nabla\widetilde{\varphi}| + \overline{s}_{\chi_\varphi} \tag{3}$$

where $\mathcal{D}$ is the molecular diffusivity of φ. The SGS mixture fraction dissipation rate appearing in the Z_v balance equation is expressed using a linear relaxation closure,

$$\overline{s}_{\chi_Z} = \frac{\overline{\rho}Z_v}{\Delta^2/\nu_T} \tag{4}$$

with Δ the local filter size and ν_T the SGS eddy viscosity. For Y_c, the progress of reaction, the dissipation rate expression that accounts for the presence of thin flame fronts is used [2]:

$$\overline{s}_{\chi_{Y_c}} = (1-S_c)\frac{\overline{\rho}(\widetilde{Y^2}-\widetilde{Y}^2)}{\Delta^2/\nu_T} + S_c\left(-\overline{\rho}\mathcal{D}|\nabla\widetilde{Y}_c|^2 + \overline{Y_c\dot{\omega}}_{Y_c} + \overline{Y_c^{Eq}\dot{\omega}}_{Y_c}/2\right) \tag{5}$$

with $S_c = (\overline{c^2}-\overline{c}^2)/(\overline{c}(1-\overline{c}))$, the unmixedness of the progress variable ($S_c \in [0,1]$), $\dot{\omega}_{Y_c}$ denotes the chemical source of Y_c. The first term in Eq. (5) accounts for low unmixedness levels, corresponding to quasi-Gaussian SGS pdfs, the second results from the BML theory [17], where the flame is seen as a thin interface separating fresh and burnt gases, with bi-modal pdfs. Once $\varphi^{FPI}(Z,c,K)$ and $\overline{P}(K^*;\underline{x},t)$ have been prescribed, all relevant thermochemical quantities and filtered sources are computed from Eq. (1), which is tabulated as functions of $\widetilde{Z}$, $S_Z = Z_v/(\widetilde{Z}(1-\widetilde{Z}))$, $\widetilde{Y}_c$ and S_c, over a non-uniform grid of $100 \times 20 \times 100 \times 20$ points, clustered around the stoichiometric surface.

As alluded above, in the experiment by Ahmed *et al* [1] some peculiar flame behavior, as a strong intermittency in ignition success in the central recirculation zone, was attributed

to strain rate effects acting on flame propagation in a fuel rich mixture zone ($Z > 0.08$, equivalence ratio slightly above 1.6), thus for conditions at which flame speed is quite sensitive to burning reduction induced by strain rate. To further examine this point, two kind of simulations are performed, with and without accounting for the impact of flame stretch on SGS tabulated chemistry. In the first, the stretch effect is neglected and $\varphi^{FPI}(Z, c, K) = \varphi^o(Z, c)$ is built from a collection of freely propagating unstrained premixed flamelets, computed with the PREMIX software [16] and the GRI methane-air detailed mechanism [21] with complex transport properties, as in previous LES using similar SGS modeling [2, 8]. In the second, the stretch is accounted for in a global manner; the starting point is based on observations by Bradley *et al.* [19], who have reported that the premixed flame response used to tabulate chemistry, as, $\dot{\omega}_q(Z, c, K)$, the volumetric heat release rate at a stretch rate, K, can be related to $\dot{\omega}_q^o(Z, c)$, the value at zero stretch rate:

$$\dot{\omega}_q(Z, c, K) = f(K)\dot{\omega}_q^o(Z, c) \tag{6}$$

where $f(K)$ is a flame stretch factor. A relation that is applied to every equivalence ratio and in the context of Eq. (2), this would read:

$$\left(\overline{\dot{\omega}_q|Z^*}\right) = \left(\overline{\dot{\omega}_q^o|Z^*}\right) P_b \tag{7}$$

with

$$P_b = \int_{K-}^{K+} f(K^*)\overline{P}(K^*; \underline{x}, t)dK^* \tag{8}$$

A thorough analysis of $f(K)$ and of the burning rate factor P_b, is given in [18], where it is shown that it behaves as

$$f(K) = 1 - \sigma K \tag{9}$$

where σ combines various flame properties, as the Markstein length, the flame thickness and flame speed. In Reynolds averaging context and assuming a Gaussian distribution for $\overline{P}(K^*; \underline{x}, t)$, the burning probability factor, P_b, response versus stretch is non-linear [18]. This is transposed to LES with three observations; first, Direct Numerical Simulation (DNS) have shown that the highest rate of strain and flame curvature result from large eddies [22], which are mostly resolved in LES; second, the zones where flame stretch is likely to impact on ignition probability have been reported in Ahmed experiment [23] to be mainly fuel rich, flamelets in the rich zone have low flame speed levels, high sensitivity to stretch and then are quenched for much smaller K levels than under stoichiometric conditions; third, laminar flame analysis demonstrates a first order linear flame response of a scaled mass burning rate versus stretch [24, 25]. From these observations, only the first order linear part is kept to correct the flamelet response to LES resolved stretch, $P_b \approx \left(1 - \mathcal{K}(\widetilde{Z})\right)$ and Eq. (7) is cast in:

$$\left(\overline{\dot{\omega}_q|Z^*}\right) = \left(\overline{\dot{\omega}_q^o|Z^*}\right)\left(1 - \mathcal{K}(\widetilde{Z})\right) \tag{10}$$

to globally correct the conditional burning rate, according to flame response to stretch, where $\mathcal{K}(\widetilde{Z})$ remains to be defined. An estimation of $\mathcal{K}(\widetilde{Z})$ is now discussed.

The steady premixed laminar flamelets equation may be written:

$$\frac{\partial \rho u \varphi}{\partial \xi} = \frac{\partial}{\partial \xi}\left(\rho \mathcal{D}_\varphi \frac{\partial \varphi}{\partial \xi}\right) + \rho \dot{\omega}_\varphi - \rho \dot{S}_{K_\varphi} \tag{11}$$

where u is the velocity, $\mathcal{D}_\varphi$ is the diffusion coefficient of φ and $\dot{\omega}_\varphi$ is the chemical source. The coordinate in the direction normal to the flame front is ξ and $\dot{S}_{K_\varphi}$ is a stretch leakage term that includes all fluxes occurring along the flame surface, thus representative of transverse convection and diffusion resulting from straining and curvature of the flamelet surface; the case of a freely propagating one-dimensional unstrained premixed flame corresponds to $\dot{S}_{k_\varphi} = 0$.

Integrating Eq. (11) in the direction normal to an unstretched flamelet ($\dot{S}_{k_\varphi} = 0$) and for $\varphi = c$, gives the relation between the unstrained flame speed S_L^o and the integral of the burning rate through the flame:

$$\begin{aligned} \rho_o(Z) S_L^o(Z) = \rho_b^o(Z) u_b^o(Z) &= \int_{-\infty}^{+\infty} \rho(Z;\xi) \dot{\omega}_c^o(Z;\xi) d\xi \\ &= \int_0^1 \rho(Z,c^*) \frac{\dot{\omega}_c^o(Z,c^*)}{|\nabla_\xi c^*|} dc^* \end{aligned} \tag{12}$$

where ρ_o is the density in the fresh gases, and, ρ_b^o and u_b^o denote the density and velocity of burned gases in the unstretched flamelet. A similar integration of Eq. (11) is done for the stretched flame, assuming a linear dependance between the stretch leakage term and the local stretch measure [24, 25, 26, 27, 28], $\dot{S}_{k_c} = Kc$, then

$$\rho_b(Z) u_b(Z) = \int_{-\infty}^{+\infty} \rho(Z;\xi) \dot{\omega}_c(Z;\xi) d\xi - \int_{-\infty}^{+\infty} \rho(Z;\xi) c(Z;\xi) K(Z;\xi) d\xi \tag{13}$$

In a more detailed analysis (see for instance [26]), the mass flux burning rate is determined at the position ξ_o on the burnt gas side of the flame. The LHS of Eq. (13) becomes $\rho(Z;\xi_o)u(Z;\xi_o)$, with ξ_o the position where the burning rate is of the order of 10% of its maximum level; to demonstrate that $\rho_b(Z)u_b(Z) \approx \rho(Z;\xi_o)u(Z;\xi_o)$ [26], mainly because the remaining contribution in burned gases remains small compared to the flame one in the range $\xi \in [0, \xi_o]$.

Further assuming that the unstretched burning rate and progress variable profiles can be used also in the integrals of the stretched relation (13), combining Eqs. (12) and (13):

$$\rho_b(Z) u_b(Z) = \rho_o(Z) S_L^o(Z) \left(1 - \frac{1}{\rho_o(Z) S_L^o(Z)} \int_{-\infty}^{+\infty} \rho(Z;\xi) c(Z;\xi) K(Z;\xi)\right) d\xi \tag{14}$$

which may be written

$$\rho_b(Z)u_b(Z) = \rho_o(Z)S_L^o(Z)\left(1 - Ka(Z)\right) \tag{15}$$

with Ka, the Karlovitz integral value computed from unstretched profiles:

$$Ka(Z) = \frac{1}{\rho_o(Z)S_L^o(Z)} \int_{-\infty}^{+\infty} \rho(Z;\xi)K(Z;\xi)c(Z;\xi)\, d\xi \tag{16}$$

From above relations, one may then write:

$$\int_{-\infty}^{+\infty} \rho(Z;\xi)\dot{\omega}_c(Z;\xi)d\xi = (1 - Ka(Z)) \int_{-\infty}^{+\infty} \rho(Z;\xi)\dot{\omega}_c^o(Z;\xi)d\xi \tag{17}$$

Arguing that flame integrated and filtered burning rates behave similarly versus stretch, this last relation may be written for the energy source:

$$\left(\overline{\dot{\omega}_q|Z^*}\right) = (1 - Ka(Z^*))\left(\overline{\dot{\omega}_q^o|Z^*}\right) \tag{18}$$

which is similar to Eq. (10), but obtained in a slightly different context. Furthermore, assuming that there exists a stretch measure Ψ_K so that

$$\int_{-\infty}^{+\infty} \rho(Z;\xi)K(Z;\xi)c(Z;\xi)\, d\xi = \Psi_K \mathcal{I}_c(Z) \tag{19}$$

with

$$\mathcal{I}_c(Z) = \int_{-\infty}^{+\infty} \rho(Z,\xi)c(Z,\xi)d\xi \tag{20}$$

the relations (10), (16), (18) and (19) lead to:

$$\mathcal{K}(\widetilde{Z}) = \frac{\mathcal{I}_c(\widetilde{Z})}{\rho_o(\widetilde{Z})S_L(\widetilde{Z})}\Psi_K \tag{21}$$

with $\mathcal{I}_c(\widetilde{Z})$ computed from the flamelet database. The stretch measure Ψ_K, may then be seen as the resolved part of the normalized time evolution of the flame surface density [29]:

$$\Psi_K = \nabla \cdot \widetilde{\mathbf{u}} - \mathbf{nn}{:}\nabla\widetilde{\mathbf{u}} + S_L\nabla \cdot \mathbf{n} \tag{22}$$

with $\mathbf{n} = -\nabla\overline{c}/|\nabla\overline{c}|$. Simulations have been performed with and without the curvature term $S_L\nabla \cdot \mathbf{n}$ in Ψ_K, without much net impact on burner ignition probability, therefore presented results are without the curvature term, which overall has a small impact on the global burning rate compared to stretch, as previously reported [30, 31, 32, 33]. Equation (10) then reads:

$$\left(\overline{\dot{\omega}_q|Z^*}\right) = \left(\overline{\dot{\omega}_q^o|Z^*}\right)\left(1 - \zeta(\widetilde{Z})\Psi_K\right) \tag{23}$$

with the following options for ζ:

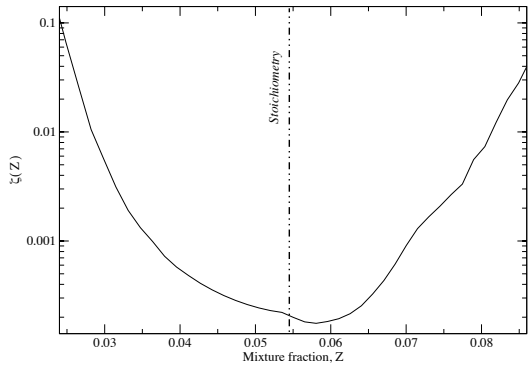

Figure 1: $\zeta(Z)$ as defined in Eq. (24).

- with $\zeta = 0$, simulations are performed without any attempt to include stretch effects on laminar flamelet speed, as it was done so far in PCM modeling [2, 8];
- with

$$\zeta(\widetilde{Z}) = \frac{\mathcal{I}_c(\widetilde{Z})}{\rho_o(\widetilde{Z}) S_L(\widetilde{Z})} \tag{24}$$

  which is a fixed distribution computed from the flamelet database, simulations are performed including an approximate stretch correction. $\zeta(\widetilde{Z})$ is plotted in Fig. 1, its minimum is found close to stoichiometry for slightly rich mixtures, and it rapidly increases in both fuel lean and rich sides. For moderate stretch levels, this first order linear attenuation has almost no impact on stoichiometric mixtures, but a non-negligible one for fuel lean and rich conditions; for example at $Z \approx 0.08$, the rich sparking condition considered in the simulations, $\zeta^{-1} = 200$ s^{-1}.

There is no adhoc constant or parameter introduced in this stretch correction, since ζ is computed from the flamelet library with Eq. (24); transposing the detailed analysis by Bradley *et al.* [18], quenching would be assumed when $\Psi_K > \zeta(\widetilde{Z})^{-1}$, it is also postulated that the inherent instability of a flame to negative stretch might cause it to reorientate toward positive stretch rate [18]. Simulations are performed at first for all cases with $\zeta = 0$, then additional simulations are conducted to evaluate the impact of the stretch correction. As expected from experimental results, it is reported thereafter that fuel rich flow locations, with high velocity fluctuations, need to be addressed with non-zero ζ to reproduce ignition variability; nevertheless, the stretch correction was not found to modify ignition probability at other locations. In addition, considering a single fuel rich location, the stretch correction does not always prevent ignition at this point, depending on turbulence properties time history; hence, ensuring that the included strain rate effect does not behave as an artificially high damping of the energy source, that would prevent

burner ignition always for rich sparking locations. The modeling of the flame kernel resulting from sparking is discussed in [34], where further details concerning the present work may also be found.

3 LES OF SPARK IGNITION

It was reported in Ahmed's experiments that the ignition kernel could get quenched by local flow fluctuations. Typically, inside the central recirculation zone where the mixture is relatively rich, there exists a considerable difference between the flammability map (probability to observe a mixture having a fuel/air ratio favorable to ignition) and the ignition probability map. Inside the CRZ, the axial velocity always plays a positive role by transporting the kernel in the negative axial direction, but still the ignition kernel fails to develop and fully lighten the burner. The velocity fluctuations inside the CRZ are quite intense and the premixed flame propagation speed in the rich mixture prevailing inside the CRZ, is several times smaller than the stoichiometric mixture, making the kernel more sensitive to the local turbulence, which can eventually quench the small burning zone, as attributed by the experimental findings. The correction proposed in Eq. (18) for stretch is activated with non-zero ζ and the LES response for various sparking point is analyzed.

The first spot (referred hereafter as point E) selected to analyse the proposed strain correction is located in a region inside the CRZ, where the flammability is high (larger than 85%), the axial velocity is negative and the mixture is quite rich. In the experiment, it was found that the ignition probability and the probability of successful flame kernel initiation were identical at this location. In other words, when the sparking results in the generation of a visible burning region that can survive long enough, then the full ignition turns out to be successful, because the ignition kernel is never convected downstream by the axial component of velocity. In contrary, when the flame kernel is quenched for the same sparking point, it happens at the very first stages of its development, when its diameter is still less than 3 mm [1].

The time history for this ignition spot (Fig. 2) confirms that in the LES, the conditions are favourable for ignition and kernel development at most of the time instants. The two time instants analysed in this case are $t_s = 0.1321$ s and $t_s = 0.13765$ s, which resulted in a quenched kernel and a successful ignition, respectively. It is to be noted that the mixture fraction during both of these time instants is relatively rich, even though it is within the flammability limit.

Figure 3 shows the evolution of the flame kernel during the unsuccessful time instance, resulting in kernel quenching. The streamline issued from the spark location confirms that the tendency of the kernel will be to travel toward the bluff-body. This is what is observed; the spark develops first into a round kernel (0.2 ms), which gets displaced through the CRZ, where the mixture remains appreciably rich with a mean mixture fraction value of about 0.08. The correction factor, $\zeta(\widetilde{Z})$, applied to the filtered burning rate is quite high for this equivalence ratio (Fig. 1). This high value of $\zeta(\widetilde{Z})$ combined with the high stretch rate, Ψ_K, induced by local turbulence, has a negative impact on the kernel development.

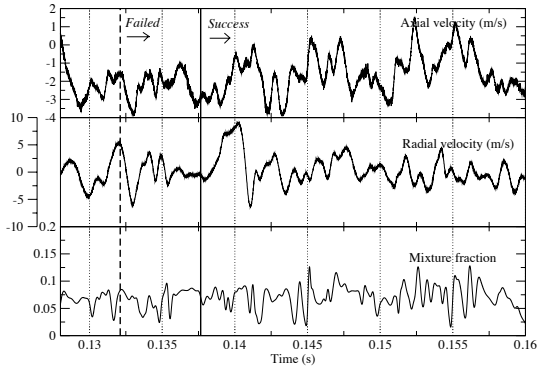

Figure 2: Time history of velocities and Mixture fraction at spot E (z = 20 mm, r = 0 mm).

From Fig. 3, it can be observed that at 1 ms after sparking, the kernel has shrunk in its size due to local high turbulence. After 5 ms, the kernel is quenched with no more sign of positive development. It is to be noted here that the observed displacement of the flame kernel is only due to the flow advection and not due to flame propagation. (The kernel would have disappeared remaining in the same position, if the time averaged velocities would have been zero.)

Figure 4 shows the successful evolution of an ignition kernel at the same point E, but at a different time instant as marked in Fig. 2. The streamline emanating from the ignition spot is not very different from the previous case, where the kernel got quenched. However, the local mixture fraction during the sparking moment is about 0.07, which is leaner than the previous case; the reduction in burning rate due to flow straining is then 10 times smaller than for $Z = 0.08$ (Fig. 1). From Fig. 4, after 1 ms, the spark kernel appears much bigger, although the local strain rate correction is still applied to the source terms (Eq. (18)).

The experimental reporting are thus reproduced, where the kernel exhibits a serious reduction in size after 1 ms, in the cases where quenching is observed. In the experiment, for the successful test cases, after 1 ms, the kernel size remains either the same, or sometimes slightly bigger (Fig. 23 of [1]). The same behaviour is observed in this LES in Figs. 3 and 4. The further global evolution of the kernel for the successful time instance is very similar to what is obtained at point C, because the convective field in the CRZ is similar; though, there is a definite reduction of the rate of the kernel growth due to the introduction of the strain correction, which increases the time taken by the kernel to fully lighten the burner.

To quantify the complete flame establishment duration, the time evolution of the volume averaged source term of energy is introduced. This quantity is displayed in Fig. 5 for point E. For the successful case, the volume averaged source term shows a linear and slow growth until 25 ms. Between 20 and 30 ms, strong reaction zones are visible near the

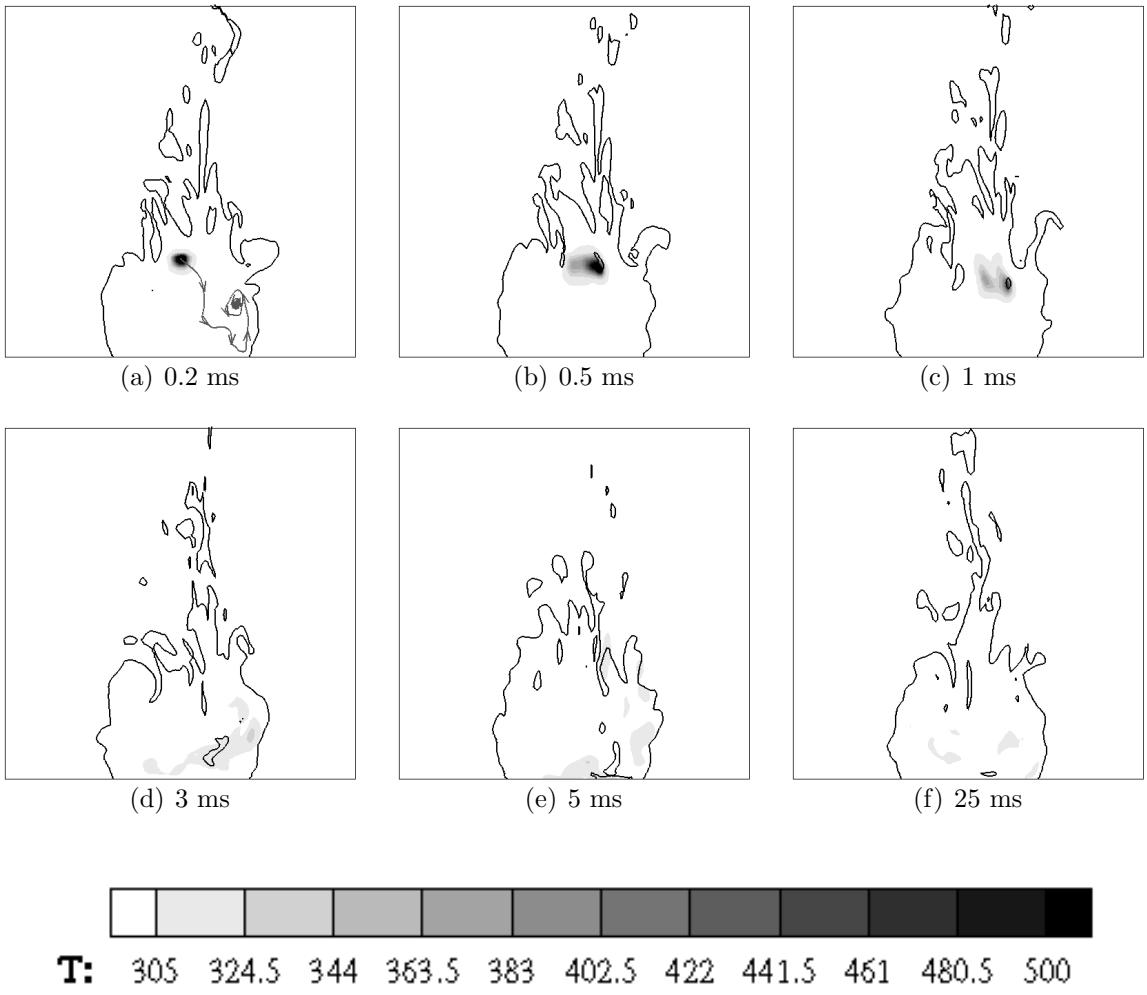

Figure 3: LES resolved instantaneous snapshots of temperature after sparking at spot E (z = 20 mm, r = 0 mm), showing kernel quenching. Sparking time = 0.1321 s. Solid black line: Iso-line of stoichiometric mixture fraction. Image shows the domain dimension of 70 x 70 mm. Time is the relative time after the ignition event.

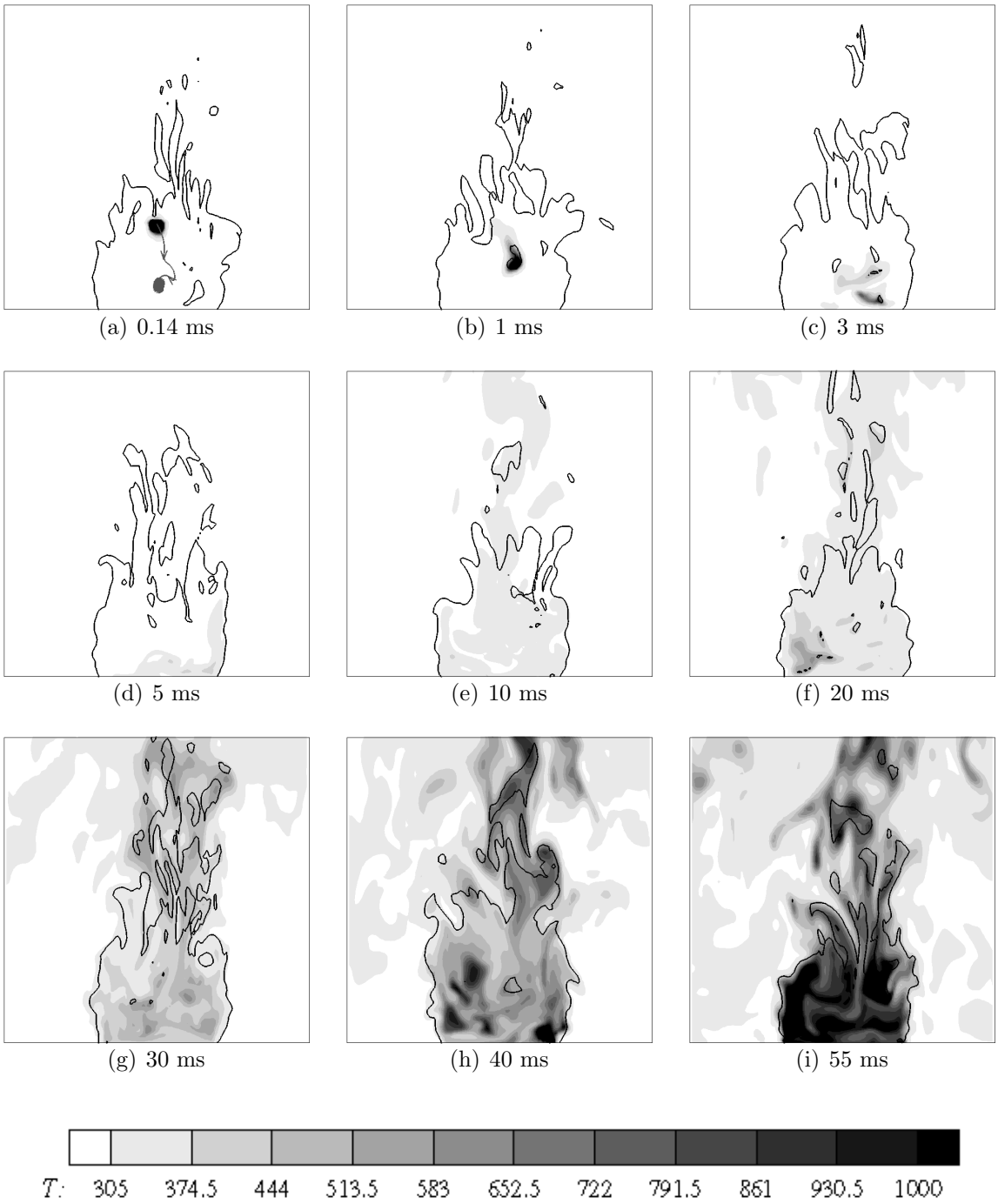

Figure 4: LES resolved instantaneous snapshots of temperature after sparking at spot E (z = 20 mm, r = 0 mm), showing positive kernel development. Sparking time = 0.13765 s. Solid black line: Iso-line of stoichiometric mixture fraction. Image shows the domain dimension of 70 x 70 mm, in caption the relative time after the ignition event.

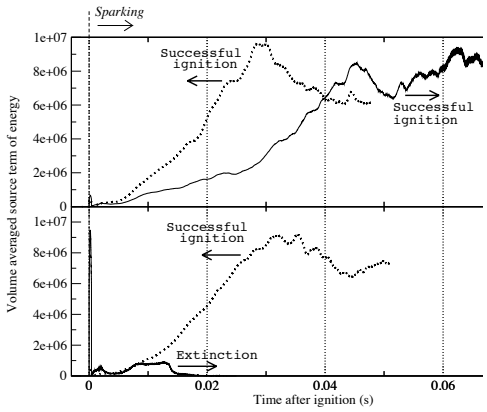

Figure 5: Time evolution of volume averaged energy source term for both successful and unsuccessful case for spot E (z = 20 mm, r = 0 mm). Time shows the relative time after sparking instance. Black dotted line: Conventional PCM-FPI closure without accounting flow straining effects, Black solid line: New closure accounting flow straining effects.

iso-stoichiometric surface (Fig. 4), which eventually accelerates the burning. Meanwhile, the temperature inside the CRZ increases, viscosity also increases and thus damps the fluctuations, thereby accelerating the burning rate. Between 25 to 50 ms, the burning rate shows a steep increase due to the tangential flame spreading through the stoichiometric mixture, noticed by the stiff slope of the evolution of total energy source term, as seen in Fig. 5. The kernel evolution observed in this case closely matches with the experimental finding in a spot inside the CRZ (Fig. 15 of [1]). The time taken for complete lightening of the burner for this case was found to be around 50 ms, in close agreement with the experiment. Fig. 5 also shows the source term evolution of the quenched case at this same ignition spot, due to local flow straining. The very quick disappearance of the flame kernel is clearly observed, only the peak corresponding to the energy deposited by the spark is visible. The volume averaged source term of energy is also plotted for a spark at the same instant ($t_s = 0.1321$ s), when the original PCM-FPI approach is employed without accounting for stretch correction. It is observed (Fig. 5 bottom) that a full lightening of the burner is obtained with this closure. More, in the simulations featuring the original approach ($\zeta = 0$ in Eq. 23), it has proved impossible to obtain a quenched kernel at Point E, whatever the time instant tested and the corresponding local conditions.

According to results discussed above, the stretch rate correction (Eq. (18)) captures the slow down of flame kernel development and the variability of ignition, as it was shown for point E, where both ignition or quenching can be found with this correction. It has

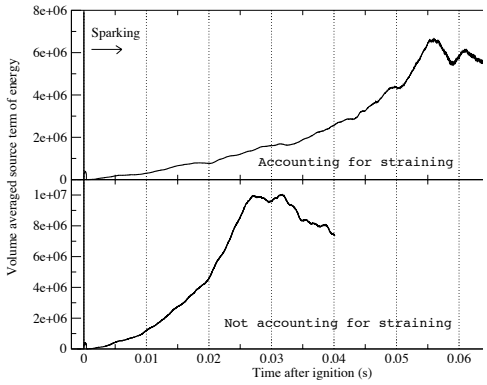

Figure 6: Time evolution of volume averaged source term with and without accounting for flow straining effects. The ignition spot D (z = 15 mm, r = 17 mm) is located on iso stoichiometric surface. Time is the relative time after sparking instance

also been verified on all previously tested points (A to D) and sparking time instants, that the success or failure of the spark to ignite the burner is not affected by the improved model. This is expected since the correction brought by Eq. (18) stays negligible for flame development arising mostly over stoichiometric mixture.

In some cases, there is a non negligible difference in the rate of flame kernel development, between the simulations with and without flow straining effects. To illustrate the reduction in burning rate, two simulations with $\zeta = 0$ (no stretch effect) and non-zero ζ (stretch as given by Eq. (18)) are performed from the same initial conditions for the ignition spots D ($z = 15$ mm, $r = 17$ mm) and E ($z = 20$ mm, $r = 0$ mm) at time instants where ignition is successful for both approaches. The time evolution of the integrated energy source term is displayed in Fig. 6 at point D, starting from the sparking instant. Without accounting for strain, intense burning starts rapidly after the spark, the total establishment time is about 30 to 40 ms. Accounting for flow straining effects, the flame establishment duration is between 55 to 70 ms. This difference predominantly arises from the initial part of the kernel development period, which is much slower in the case accounting for strain effects, the reduction in burning rate attributed to the flow straining is thus dominant for young flame kernel. A similar lengthening of the flame establishment time is observed for point E in Fig. 5 top. This is the reason why the kernels are often quenched when the sparking is inside the CRZ (for instance point E discussed before), since at this location, they face high turbulence levels while being of small size. A parallel can be made with experimental observations, which concluded that a young kernel is more prone to

quench compared to a developed one, for the same turbulence intensity [35]. Therefore, if an ignition kernel can sufficiently grow before being inducted into highly strained and rich mixtures within the CRZ, it is not quenched. This has been observed for spot ignition D, when the kernel has grown substantially by spreading through the stoichiometric surface, before entering the recirculation zone to promote full ignition of the burner.

4 SUMMARY

Large Eddy Simulation of spark ignition was performed using tabulated detailed chemistry. Comparing with experimental measurments shows that intense strain rate effects cannot be neglected in chemistry modeling, specifically when sparking in fuel rich (or lean) zones. A correction function to usual flamelet modeling was proposed and tested to account for such high flow straining.

ACKNOWLEDGMENTS

Financial support by the European Commission through the project 'Toward Innovative Methods for Combustion Prediction in Aeronautic Engines" (TIMECOP-AE, AST5-CT-2006-030828) is gratefully acknowledged. The authors extend their kind acknowledgement to Dr. Ahmed and Prof. Mastorakos of Cambridge University, UK for providing the experimental data for comparison and for many fruitful discussions. The computational resources were provided by CRIHAN (Haute Normandie) and GENCI - IDRIS (CNRS).

REFERENCES

[1] S. F. Ahmed, R. Balachandran, T. Marchione, and E. Mastorakos. Spark ignition of turbulent nonpremixed bluff-body flames. *Combust. Flame*, 151:366–385, 2007.

[2] P. Domingo, L. Vervisch, and D. Veynante. Large-eddy simulation of a lifted methane jet flame in a vitiated coflow. *Combust. Flame*, 152:415–432, 2008.

[3] F. Ducros, F. Laporte, T. Souleres, V. Guinot, P. Moinat, and B. Caruelle. High-order fluxes for conservative skew-symmetric-like schemes in structured meshes: application to compressible flows. *Journal of computational physics*, 161:114–139, 2000.

[4] A. A. Wray. Minimal storage time-advancement schemes for spectral methods. Computational fluid dynamics branch, NASA Ames research centre, Moffett Field, CA 94035, 1986.

[5] M. Klein, A. Sadiki, and J. Janika. A digital filter based generation of inflow data for spatially developing direct numerical or large eddy simulations. *Journal of Computational Physics*, 186:652–665, 2003.

[6] T. J. Poinsot and S. K. Lele. Boundary conditions for direct simulations of compressible viscous flow. *Journal of computational physics*, 101:104–129, 1992.

[7] J. Smagorinsky. General circulation experiments with the primitives equations. *Mon. Weather Rev.*, 61:99–164, 1963.

[8] J. Galpin, A. Naudin, L. Vervisch, C. Angelberger, O. Colin, and P. Domingo. Large-eddy simulation of a fuel-lean premixed turbulent swirl-burner. *Combust. Flame*, 155:247–266, 2008.

[9] L. Vervisch, P. Domingo, M. Rullaud, and R. Hauguel. Three facets of turbulent combustion modelling: DNS of premixed v-flame, LES of lifted nonpremixed flame and RANS of jet-flame. *Journal of turbulence*, 5:1–36, 2004.

[10] B. Fiorina, O. Gicquel, L. Vervisch, S. Carpentier, and N. Darabiha. Premixed turbulent combustion modeling using tabulated detailed chemistry and pdf. *Proc. Combust. Inst*, 30:867–874, 2005.

[11] P. Domingo, L. Vervisch, S. Payet, and R. Hauguel. DNS of a premixed turbulent v flame and LES of a ducted flame using a FSD-PDF subgrid scale closure with FPI-tabulated chemistry. *Combust. Flame*, 143:566–586, 2005.

[12] A. W. Vreman, B. A. Albrecht, J. A. van Oijen, and R. J. M. Bastiaans. Premixed and nonpremixed generated manifolds in large-eddy simulation of sandia flame d and f. *Combust. Flame*, 153(3):394–416, 2008.

[13] B. Fiorina, O. Gicquel, L. Vervisch, S. Carpentier, and N. Darabiha. Approximating the chemical structure of partially premixed and diffusion counterflow flames using fpi flamelet tabulation. *Combust. Flame*, 140(3):147–160, 2005.

[14] O. Gicquel, N. Darabiha, and D. Thevenin. Laminar premixed hydrogen/air couter-flow flame simulations using flame prolongation of ildm with differential diffusion. *Proc. Combust. Inst.*, 28:1901–1908, 2000.

[15] J. A. van Oijen, F. A. Lammers, and L. P. H. de Goey. Modeling of complex premixed burner systems by using flamelet-generated manifolds. *Combust. Flame*, 127(3):2124–2134, 2001.

[16] R. J. Kee, J. F. Gracer, M. D. Smooke, and J. A. Miller. A fortran program for modeling steady laminar one-dimensional premixed flames. Technical report, Report no - Report No. SAND87-8248 UC-4, Sandia National Laboratories, 1990.

[17] K. N. C. Bray. The challenge of turbulent combustion. *Proc. Combust. Inst.*, 26:1–26, 1996.

[18] D. Bradley, P. H. Gaskell, and X. J. Gu. The modeling of aerodynamic strain rate and flame curvature effects in premixed turbulent combustion. *Twenty-Seventh Symp. (Int.) on Combustion*, 27:849–856, 1998.

[19] D. Bradley, P. H. Gaskell, X. J. Gu, and A. Sedaghat. Premixed flamelet modeling: factors influencing the turbulent heat release rate source term and the turbulent burning velocity. *Combust Flame*, 143(3):227–245, 2005.

[20] L. Vervisch, G. Lodato, and P. Domingo. *Quality and Reliability of Large-Eddy Simulations*, chapter Reliability of Large-Eddy Simulation of Nonpremixed Turbulent Flames: Scalar Dissipation Rate Modeling and 3D-Boundary Conditions, pages 227–237. Number ISBN:978-1-4020-8577-2. Springer Netherlands, 2008.

[21] G. P. Smith, D. M. Golden, M. Frenklach, N. W. Moriarty, B. Eiteneer, M. Goldenberg, C. T. Bowman, R. K. Hanson, S. Song, W. C. Gardiner, V. V. Lissianski, and Z. Qin. Technical report, 1999. http://www.me.berkeley.edu/gri-mech/.

[22] T. Poinsot. Using direct numerical simulations to understand premixed turbulent combustion. In *Proceedings of the 26th Symp. (Int.) on Combustion. The Combustion Institute, Pittsburgh.*, pages 219–232, 1996.

[23] S. F. Ahmed. *Spark Ignition of Turbulent Non-premixed Flames*. PhD thesis, University of Cambridge, September 2006.

[24] S. H. Chung and C. K. Law. An integral analysis of the structure and propagation of stretched premixed flames. *Combust. Flame*, 72(3):325–336, 1988.

[25] P. Clavin. Premixed combustion and gasdynamics. *Annu. Rev. Fluid Mech.*, 26:321–52, 1994.

[26] L. P. H. de Goey and J. H. M. ten Thije Boonkkamp. A flamelet description of premixed laminar flames and the relation with flame stretch. *Combust. Flame*, 119:253–271, 1999.

[27] L. P. H. de Goey, R. M. M. Mallens, and J. H. M. ten Thije Boonkkamp. An evaluation of different contributions to flame stretch for stationary premixed flames. *Combust Flame*, 110:54–66, 1997.

[28] J. A. M. de Swart, G. R. A. Groot, J. A. van Oijen, J. H. M. ten Thije Boonkkamp, and L. P. H. de Goey. Detailed analysis of the mass burning rate of stretch flames including preferential diffusion effects. *combust. Flame*, 145:245–258, 2006.

[29] T. Poinsot and D. Veynante. *Theoretical and Numerical Combustion*. R. T. Edwards, Inc., 2005.

[30] J. H. Chen and H. G. Im. Correlation of flame speed with stretch in turbulent premixed methane/air flames. *Twenty-Seventh Symposium (International) on Combustion. The Combustion Institute*, pages 819–826, 1998.

[31] C. J. Mueller, J. F. Driscoll, D. L. Reuss, and M. C. Drake. Effects of unsteady stretch on the strength of a freely propagating flame wrinkled by a vortex. *Twenty-Sixth Symposium (International) on Combustion/The Combustion Institute*, pages 347–355, 1996.

[32] I. F. Huang, S. S. Shy, C. C. Chang, S. C. Li, and C. M. Huang. Spatiotemporal measurements of flame stretch and propagation rates for lean and rich ch4/air premixed flames interacting with a turbulent-wake. *Proceedings of the Combustion Institute*, 32:1755–1762, 2009.

[33] M. Z. Haq, C. G. W. Sheppard, R. Woolley, D. A. Greenhalgh, and R. D. Lockett. Wrinkling and curvature of laminar and turbulent premixed flames. *Combust. Flame*, 131:1–15, 2002.

[34] V. Subramanian, P. Domingo, and L. Vervisch. Large-eddy simulation of forced ignition of an annular bluff-body burner. *Combust. Flame*, 157(3):579–601, 2010.

[35] S. K. Marley, S. J. Danby, W. L. Roberts, M. C. Drake, and T. D. Fansler. Quantification of transient stretch effects on kernel–vortex interactions in premixed methane–air flames. *Combust. Flame*, 154:296–309, 2008.